

Cite this: *Dalton Trans.*, 2018, **47**, 16524

# Highly luminescent 2-phenylpyridine-free diiridium complexes with bulky 1,2-diarylimidazole cyclometalating ligands†

Daniel G. Congrave, \* Andrei S. Batsanov  and Martin R. Bryce \*

While a number of highly emissive dinuclear Ir(III) complexes have been reported, they have generally been restricted to structures based on 2-phenylpyridine (Hppy) cyclometalates. We now present a series of new hydrazide-bridged diiridium complexes (**5–8**) which incorporate bulky 1,2-diarylimidazole cyclometalating ligands in the place of Hppy. Complexes **6–8** are strongly emissive when doped into poly(methyl methacrylate) (PMMA), displaying the highest PLQYs yet reported for ppy-free diiridium emitters ( $\Phi_{\text{PL}} = 47\text{--}55 \pm 10\%$ ). Notably, complex **8** has an emission peak at 452 nm and  $\text{CI}_{\text{E}_{xy}}$  colour coordinates in the sky-blue region (0.18, 0.27), which is competitive with state-of-the-art monoiridium analogues. X-ray crystallography and solution-state  $^{19}\text{F}$  NMR spectra reveal the presence of rigidifying intramolecular  $\pi\text{--}\pi$  interactions for complexes **6–8**, which explains their improved photophysical performance compared to **5** which does not have these interactions. Structure–property relationships are further rationalised through density functional theory (DFT) and cyclic voltammetry (CV) data. All the complexes studied in this work display aggregation induced phosphorescent emission (AIPE). This series of compounds increases the structural diversity of highly luminescent dinuclear Ir(III) complexes to include luminophoric ligands that are not restricted to Hppy-type fragments. The colour range accessible to AIPE-active diiridium complexes has also been substantially broadened.

Received 8th October 2018,  
Accepted 2nd November 2018

DOI: 10.1039/c8dt04043e

rsc.li/dalton

## Introduction

Iridium(III) complexes have been extensively studied over the last 30 years.<sup>1</sup> The metal–ligand based photochemistry has enabled their emission colour to be tuned across the entire visible spectrum through modular synthesis.<sup>2</sup> They typically feature high luminescence quantum efficiencies ( $\Phi$ ), microsecond-scale phosphorescence lifetimes ( $\tau$ ) and good electrochemical stabilities. These properties are advantageous for applications<sup>3</sup> such as photocatalysis,<sup>4</sup> biological labelling,<sup>5</sup> sensing,<sup>6</sup> and phosphorescent organic light-emitting devices (PhOLEDs)<sup>7,8</sup>

Interest in phosphorescent dinuclear Ir(III) complexes has recently increased. Unlike their mononuclear analogues, they feature ligands which bridge the two metal centres. A wide variety of bridging ligands has been explored, and they can heavily influence the photophysical properties of the complexes.<sup>9–22</sup> For example, flexible bridges impart aggregation-induced phosphorescent emission (AIPE) to orange/red-

emitting complexes,<sup>14</sup> which have been employed in sensing applications.<sup>23,24</sup> Complementarily, bridging ligands can lead to rigid complexes, either covalently through the incorporation of rigid polyaromatic structures (complexes **1**, **2** and **3**, Fig. 1),<sup>15,17,18,22,25</sup> or non-covalently through promoting intramolecular perfluoroaryl–aryl  $\pi\text{--}\pi$  interactions with peripheral ligands (complex **4**, Fig. 1).<sup>26</sup> This has allowed the development of diiridium complexes that exhibit high solution photoluminescence quantum yields (PLQYs) (>ca. 50%) from the red to the sky-blue regions of the visible spectrum (e.g. complexes **1–4**). Diiridium complexes have also demonstrated advantages over their mononuclear counterparts. For example, sub-microsecond phosphorescence lifetimes are obtained alongside high PLQYs (complexes **1** and **2**) due to high radiative rate constants ( $k_r$ ), which is likely due to an improved spin–orbit coupling (SOC) effect exerted by two proximal heavy metal atoms.<sup>15,17,25</sup> Chang and co-workers have also recently reported sky-blue diiridium phosphors with unity PLQY that are sublimable.<sup>22</sup>

2-Phenylpyridine (Hppy)-based cyclometalating ligands (Fig. 1) are popular for Ir(III) phosphors due to their synthetic versatility, well-understood structure–property relationships, and because they reliably afford complexes with high PLQYs.<sup>27–29</sup> Consequently, Hppy-type fragments that form

Department of Chemistry, Durham University, South Road, Durham DH1 3LE, UK.  
E-mail: d.g.congrave@outlook.com, m.r.bryce@durham.ac.uk

† Electronic supplementary information (ESI) available: Synthetic details, NMR spectra, X-ray data. CCDC 1871136 for **7** and 1871137 for **8**. For ESI and crystallographic data in CIF or other electronic format see DOI: 10.1039/c8dt04043e

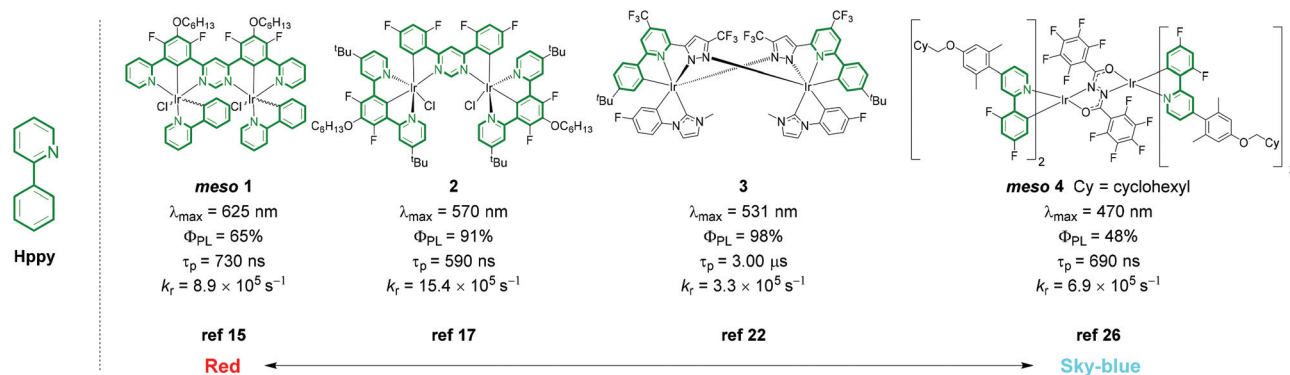


**Fig. 1** Representative highly emissive diiridium complexes containing 2-phenylpyridine (Hppy) fragments with selected solution photoluminescence parameters (all obtained in degassed DCM). 2-Phenylpyridine fragments are highlighted in green.

5-membered cyclometalates have been incorporated into the bridging or peripheral ligands of almost all the significantly emissive diiridium complexes (PLQY > ca. 30%) reported in the literature (e.g. complexes 1–4).<sup>8,9,14,16,18,20,23,25</sup> In contrast, non-Hppy components have been seldom explored in diiridium complexes. We know of only a single structural type that does not contain a Hppy fragment and is significantly emissive at room temperature: namely, cationic AIPE complexes featuring 2-(phenyl)pyrazole (Hppz) cyclometalating ligands which exhibit orange/red emission with PLQYs  $\leq 31\%$ .<sup>23,31</sup> This lack of structural diversity is restrictive, especially considering that Hppy-based cyclometalating ligands have some drawbacks. For example, the synthesis of Hppy-based ligands often requires expensive transition metal-catalysed routes.<sup>32</sup> Also Hppy-derived sky-blue/blue emissive Ir(III) complexes suffer from poor excited state stability, particularly under PhOLED operation.<sup>27</sup>

Bulky 1,2-diarylimidazole ligands which form 5-membered cyclometalates are very topical as they have afforded highly emissive sky-blue mononuclear Ir(III) complexes that are notably more stable under PhOLED operating conditions than Hppy-functionalised analogues.<sup>27,30,33–38</sup> They have also been incorporated into heteroleptic mononuclear Ir(III) complexes that show promising preferential dipole alignment in solution-processed films.<sup>30</sup> Beneficially, 1,2-diarylimidazole ligands can also be synthesised from readily available starting materials through condensation chemistry, avoiding transition metal catalysis.<sup>39</sup> Despite this promise, while 1,2-diarylimidazoles have been studied as cyclometalating ligands in homo- and heteroleptic monoiridium complexes,<sup>38,40–42</sup> to the best of our knowledge they have not previously been applied to phosphorescent diiridium systems.

The aim of the present work is to diversify phosphorescent dinuclear Ir(III) complexes to include structures that are not restricted to Hppy-based ligands. We present a series of new diiridium complexes (5–8) (Fig. 2) which feature bulky 1,2-diarylimidazole cyclometalating ligands alongside hydrazide bridging ligands. Density functional theory (DFT) calculations, X-ray crystallography and electrochemical data provide further insight into their structural and optoelectronic properties.

## Results and discussion

### Design, synthesis and characterisation

The structures of the complexes 5–8 are shown in Fig. 2. The complexes are of the formula  $[(\text{Ir}(\text{C}^{\wedge}\text{N})_2)_2(\text{O}^{\wedge}\text{N}^{\wedge}\text{N}^{\wedge}\text{O})]$  with  $\text{C}^{\wedge}\text{N} = 9\text{--}11$  and  $\text{O}^{\wedge}\text{N}^{\wedge}\text{N}^{\wedge}\text{O} = 12$  and 13. The conjugate acids of the ligands in the complexes (H9–H11 and 2H12 and 2H13) are also shown in Fig. 2. The mesityl-functionalised 1,2-diarylimidazole cyclometalating ligand H9 was selected due to the favourable photophysical properties of its homoleptic complex,<sup>30,34</sup> and because the steric bulk of the mesityl group should impart solubility and rigidity without inhibiting the formation of the complexes 5–8. The bridging ligands 2H12 and 2H13 were employed in complexes 5 and 6 to target sky-blue emission and study the effect of intramolecular  $\pi\text{--}\pi$  stacking between the perfluoroaryl groups of 12 and the peripheral cyclometalating ligands.<sup>26</sup> Due to the enhanced photophysical performance of 6 compared to 5 (discussed below) the perfluoroaryl bridge 2H12 was incorporated into complexes 7 and 8, where incremental fluorination of their cyclometalating ligands (H10 and H11) blue shifts their emission through HOMO stabilisation.

The bridging ligands 2H12 and 2H13 were synthesised as reported.<sup>26</sup> The cyclometalating ligands H9–H11 were accessible on a multi-gram scale following Strassner's one-pot transition metal-free procedure.<sup>39</sup> The diiridium complexes 5–8 were then synthesised by cleaving the corresponding  $\mu\text{-Cl}$  dimers with the bridging ligands 2H12 or 2H13 under basic conditions.<sup>12,13,19,26</sup> Complexes 6–8 were obtained in  $\geq$ ca. 50% yields as diastereomeric mixtures which were not separated, apart from complex 5, which was isolated as a single diastereomer. This follows literature precedent, where incorporation of the bis-trifluoromethyl bridge 2H13 affords diastereoselectivity.<sup>26</sup>

Complexes 5–8 show good thermal stability with decomposition temperatures ( $T_{\text{d}}$  corresponding to 5% weight loss) of  $>400 \text{ }^{\circ}\text{C}$  by thermal gravimetric analysis (TGA) (Fig. S6–S9†).

Expansions of the  $\text{C}_6\text{F}_5$  regions of the  $^{19}\text{F}$  { $^1\text{H}$ } NMR spectra of complexes 6–8 are shown in Fig. 3. The  $^{19}\text{F}$  NMR spectra for the diastereomeric mixtures of 6–8 each display 10 environments in the  $\text{C}_6\text{F}_5$  region (5 per diastereoisomer). This is

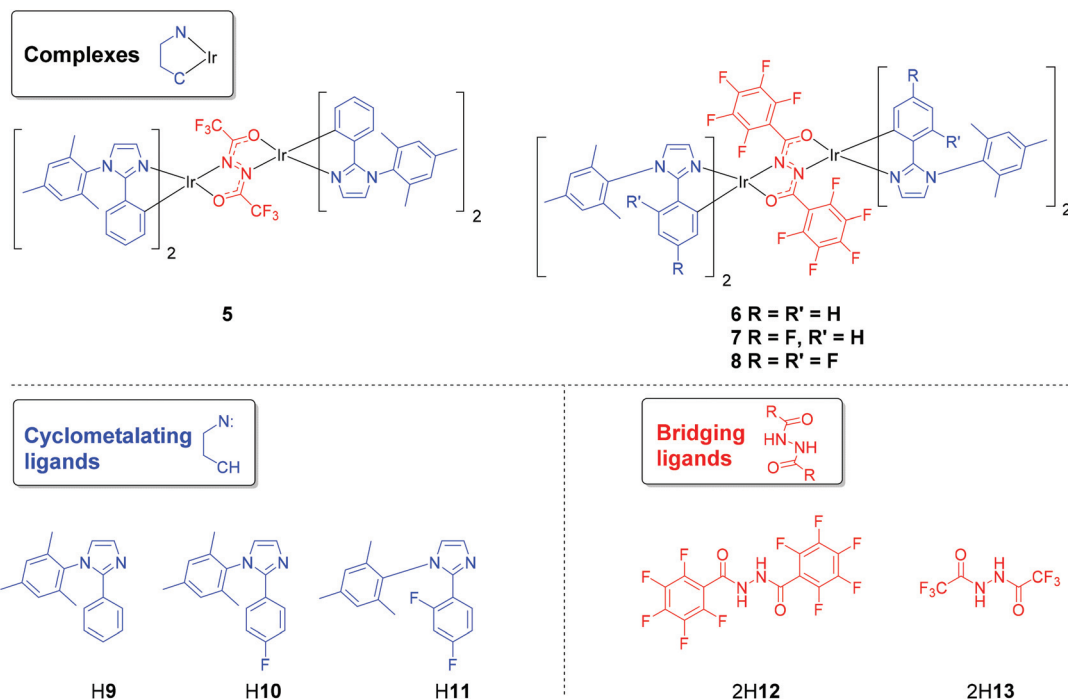


Fig. 2 Structures of the complexes and ligands studied in this work.

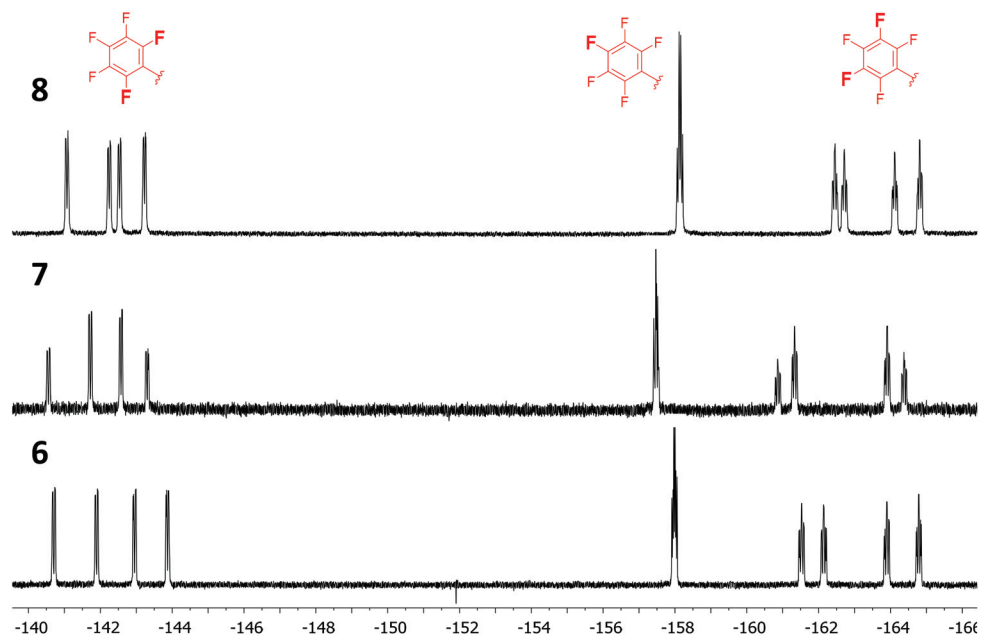
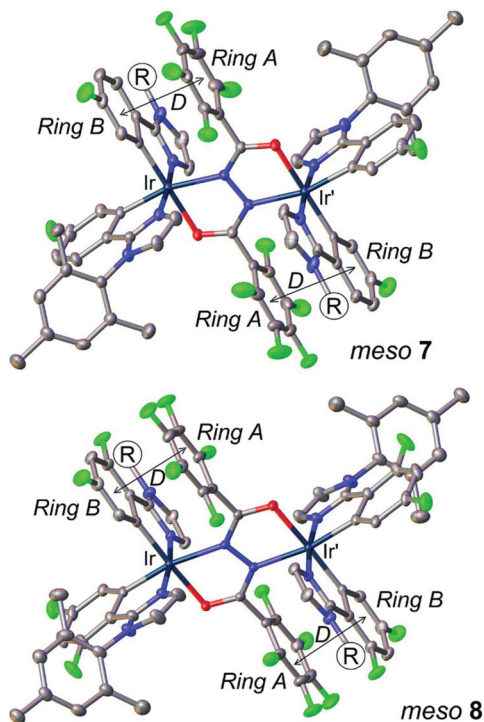


Fig. 3 Expansions of the  $C_6F_5$  regions of the 376 MHz  $^{19}F$  ( $^1H$ ) spectra of 6–8 recorded in  $CDCl_3$  at 298 K. Diastereomeric ratios from integration: 6 ca. 1 : 1, 7 ca. 1 : 0.6, 8 ca. 1 : 0.9.

greater than the 6 environments that would be expected (3 per diastereoisomer) for mono-substituted perfluorophenyl groups, and is due to a lowering of molecular symmetry. This is ascribed to restriction of rotation of the bridge  $C_6F_5$  groups due to intramolecular  $\pi$ – $\pi$  interactions with peripheral cyclometalating ligands (seen in the solid state for 7 and 8 in the X-ray diffraction data below).<sup>26,43</sup>

#### X-ray crystal structures

The single-crystal X-ray crystal structures of the *meso* diastereomers of 7 and 8 are displayed in Fig. 4. Relevant parameters are listed in Table 1. Presumably, the *meso* diastereomers preferentially crystallised from solutions of diastereomeric mixtures due to their inversion centre symmetry. *Meso* 7 crystal-



**Fig. 4** X-ray molecular structures of *meso* 7 and *meso* 8. R = mesityl. Thermal ellipsoids are drawn at the 50% probability level, H atoms, solvent of crystallisation and some mesityl groups are omitted for clarity. Primed atoms are generated by a crystallographic inversion centre. Vector *D* identifies intramolecular  $\pi$ - $\pi$  interactions (see Table 1).

**Table 1** Selected geometrical parameters of 7 and 8 (bond distances in Å)

	<i>meso</i> 7 · 6CH <sub>2</sub> Cl <sub>2</sub>	<i>meso</i> 8 · 2MeOH
Space group	<i>C2/c</i>	<i>Pbca</i>
Mol. symmetry	<i>C<sub>i</sub></i>	<i>C<sub>i</sub></i>
Ir centres	$\Delta\Delta$	$\Delta\Delta$
Ir...Ir, Å	5.022	5.065
Ir-C ( <i>trans</i> -O)	2.003(4)	2.003(3)
Ir-C ( <i>trans</i> -N)	2.012(4)	2.016(3)
Ir-N, stacked	2.020(3)	2.018(2)
Ir-N, non-stacked	2.019(3)	2.040(2)
<b>Bridge geometry</b>		
OCNNO folding, °	Planar	Planar
Ir displacement, Å	0.086	0.208
Ir-O	2.119(3)	2.130(2)
Ir-N	2.144(3)	2.159(2)
N-N	1.434(4)	1.437(3)
N-C	1.306(6)	1.305(4)
C-O	1.279(4)	1.287(3)
<b>Intramolecular stacking (<math>\pi</math>-<math>\pi</math>)</b>		
$\theta^a$ , °	3.5	3.0
$D^b$ , Å	3.30	3.26
Centroid-centroid, Å	3.35	3.41

<sup>a</sup> Interplanar angle between ring A of the bridging ligand and ring B of the cyclometalating ligand (see Fig. 4). <sup>b</sup> Distance between the plane of ring B and the centroid of ring A.

lised as a DCM hexasolvate whereas *meso* 8 crystallised as a MeOH disolvate.

The Ir centres in both structures display distorted octahedral coordination. The N atoms of the two C<sup>^</sup>N cyclometalating ligands occupy axial positions with respect to the bridge plane, and are *trans* to one another.<sup>8,12</sup> The central hydrazide moieties of *meso* 7 and *meso* 8 are planar, and the aryl substituents (A) on the bridging ligands are oriented approximately perpendicular to the hydrazide planes and are stacked face-to-face ( $\pi$ - $\pi$ ) with the phenyl ring (B) of a cyclometalating ligand (Fig. 4). The stacking is closer and more parallel in *meso* 8 compared to *meso* 7 ( $\theta$  = 3.0 vs. 3.5°,  $D$  = 3.26 vs. 3.30 Å). However, the slightly larger centroid-centroid distance for *meso* 8 (3.41 Å vs. 3.35 Å for *meso* 7) indicates greater slippage of the stacked rings.

### Electrochemical study

The oxidation and reduction processes for 5–8 were studied by cyclic voltammetry (CV). The data are listed in Table 2. The oxidative waves are presented in Fig. 5 and the reductive processes are included in Fig. S1.† All complexes display two oxidation waves.

They are assigned to sequential Ir<sup>3+</sup>/Ir<sup>4+</sup> redox couples and are indicative of electronic communication between the two centres. Both oxidations are electrochemically reversible for 5–8 based on the equal magnitudes of the coupled oxidation and reduction peaks. All reduction processes are electrochemical irreversible.

The first oxidation potential of 5 is more positive than for 6 (by 0.04 V). This suggests that the complexed bis(trifluoromethyl) bridge 2H13 is more electron withdrawing than the bis(pentafluorophenyl) bridge 2H12.<sup>44</sup> Sequential fluorination of the cyclometalating ligands in 6–8 leads to successive increases in the first oxidation potentials, as expected. The peak splitting between the first and second oxidations ( $\Delta E_{1/2}$ ) for the series 6–8 also increases incrementally, suggesting that the bridge HOMO contribution increases along the series. Complex 5 displays the lowest  $\Delta E_{1/2}$ . This is because the complexed bridge 2H13 has a shorter conjugation length than 2H12 and therefore is expected to feature a larger energy gap, decreasing its contribution to the HOMO of 5. These conclusions are corroborated by the DFT data below.

The reduction onsets for 5–8 are comparable to the values for heteroleptic mononuclear complexes functionalised with 2-arylimidazole ligands.<sup>41</sup> While the irreversible nature of the reductions hinders their accurate determination, there are two clear qualitative trends in the data. (i) The reduction potential for 5 is less negative than for 6, *i.e.* 5 is easier to reduce, in-line with the more electron-withdrawing complexed bridge 2H13 and the higher first oxidation potential of 5. (ii) Sequential fluorination in the series 6–8 leads to consecutively less negative reduction potentials as the complexes become more electron poor. However, the LUMO energies do not drop as significantly as the HOMO energies upon fluorination, leading to sequentially larger electrochemical bandgaps in the order 6 < 7 < 8.

**Table 2** Electrochemical data for complexes 5–8 referenced to  $E_{1/2}$  FcH/FcH<sup>+</sup> = 0.00 V

Complex	$E^{\text{ox}(1)}/V E_{\text{pa}}/E_{\text{pc}} [E_{1/2}]$	$E^{\text{ox}(2)}/V E_{\text{pa}}/E_{\text{pc}} [E_{1/2}]$	$\Delta E_{1/2}^a/V$	$E_{\text{onset}}^{\text{red}}/V$	HOMO <sup>c</sup> /eV	LUMO <sup>d</sup> /eV
5	0.38/0.29 [0.34]	0.65/0.55 [0.60]	0.26	−2.82	−5.14	−1.98
6	0.33/0.24 [0.30]	0.73/0.62 [0.67]	0.37	−2.95	−5.10	−1.85
7	0.55/0.43 [0.49]	0.95/0.84 [0.89]	0.40	−2.89	−5.29	−1.91
8	0.72/0.63 [0.68]	1.18/1.05 [1.12]	0.44	−2.76	−5.48	−2.04

<sup>a</sup> Peak splitting between  $E^{\text{ox}(1)}$  and  $E^{\text{ox}(2)}$ . <sup>b</sup> All reductions are electrochemically irreversible. <sup>c</sup> HOMO levels calculated from CV potentials by  $\text{HOMO} = -4.8 + (-E_{1/2}^{\text{ox}(1)})$ , using ferrocene as the standard. <sup>d</sup> LUMO levels calculated from CV potentials by  $\text{LUMO} = -4.8 + (-E_{\text{onset}}^{\text{red}})$ , using ferrocene as the standard.

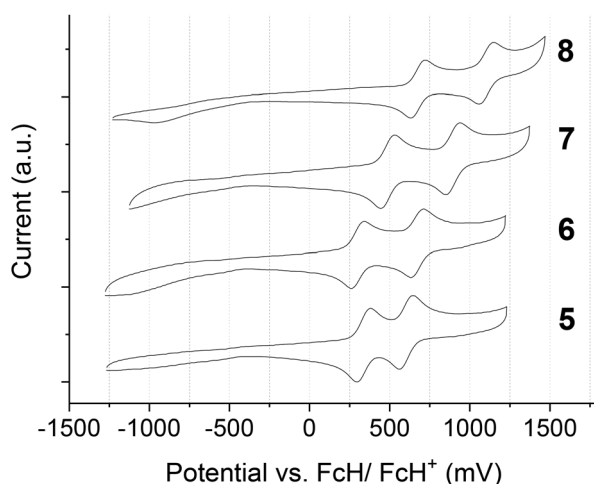


**Fig. 5** Cyclic voltammograms in 0.1 M *n*-Bu<sub>4</sub>NPF<sub>6</sub>/DCM showing the oxidation processes for complexes 5–8. The current range for each voltammogram is 10 to −10 μA.

### Photophysical properties

The absorption spectra of 5–8 are shown in Fig. S2† and the data are listed in Table S1.† The spectra display features typical of cyclometalated iridium complexes: there are intense bands below *ca.* 300 nm which correspond to population of LC states, while the weaker bands extending to *ca.* 450 nm are assigned to <sup>1</sup>MLCT and <sup>3</sup>MLCT transitions.<sup>45,46</sup> The extinction coefficients are higher than for similar mononuclear 2-phenylimidazole complexes,<sup>41</sup> ascribed to a larger number of cyclometalating ligands and Ir atoms per complex. An increase in the intensity of the <sup>3</sup>MLCT bands compared to mononuclear analogues may be due to improved spin–orbit coupling in dinuclear complexes.<sup>15,17</sup>

The emission spectra for 5–8 doped into poly(methyl methacrylate) (PMMA) at room temperature, and in 2-MeTHF at 77 K are shown in Fig. 6. Photoluminescence data are tabulated in Table 3. Complexes 5–8 are non-emissive in DCM solution at room temperature with PLQYs ≤ 0.05%. In contrast, they are emissive (PLQY = 11–55 ± 10%) in the blue-green/sky-blue regions at room temperature in dilute PMMA films (1 wt% complex). To the best of our knowledge, complexes 6–8 exhibit the highest PLQYs yet reported for ppy-free diiridium complexes (PLQY = 47–55 ± 10%).<sup>23,31</sup> Sequential fluorination of the cyclometalating ligands in the series 6–8 leads to incremental blue shifts in their emission, as expected. We note that

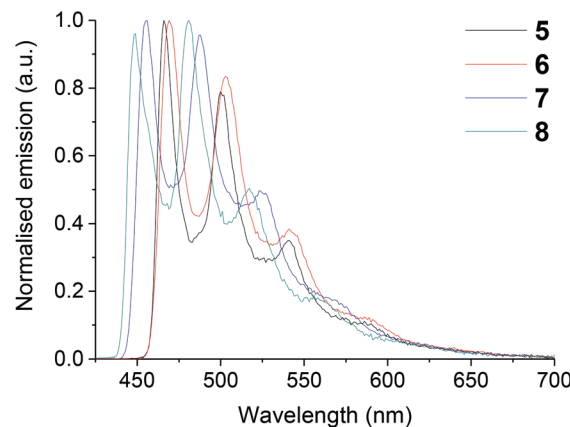
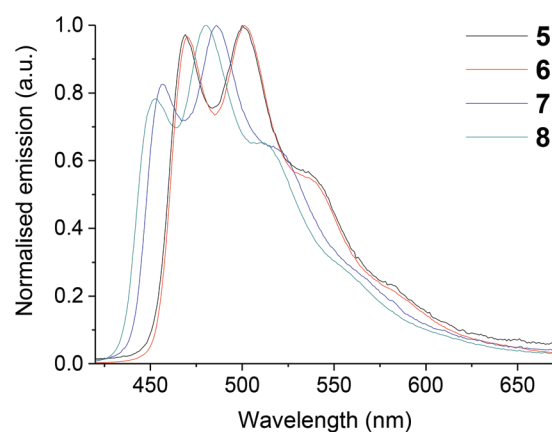


**Fig. 6** Emission spectra for complexes 5–8. (Top) Spectra of complexes doped into PMMA at 1 wt% at room temperature. (Bottom) Spectra of complexes in 2-MeTHF glasses at 77 K ( $\lambda_{\text{exc}}$  355 nm).

complex 8 has an emission peak (452 nm) and CIE<sub>xy</sub> coordinates (0.18, 0.27) that are competitive with the bluest monoiridium analogues that contain arylimidazole ligands.<sup>35,38</sup> The comparatively broad emission of 5–8 is reminiscent of mononuclear analogues.<sup>27,30,33–38</sup> While we cannot completely disregard any effects of diastereomeric mixtures on the optoelectronic properties of 6–8, there are literature precedents that diiridium diastereomers display very similar photophysical properties.<sup>15,25</sup>

The matrix-dependent emission properties of 5–8 are ascribed to non-radiative emission quenching in solution. As

Table 3 Summary of the key photoluminescence data for complexes 5–8

Complex	Doped into PMMA 1 wt% <sup>a</sup>				2-MeTHF glass <sup>b</sup>		
	$\lambda_{\text{max em/nm}}$ [CIE <sub>xy</sub> ]	PLQY/% ( $\pm 10\%$ )	$\tau/\mu\text{s}$	$k_r/\times 10^5 \text{ s}^{-1}$	$k_{\text{nr}}/\times 10^5 \text{ s}^{-1}$	$\lambda_{\text{max em/nm}}$ ( $\lambda_{10\% \text{ em/nm}}$ ) <sup>c</sup> [ $E_T/\text{eV}$ ] <sup>d</sup>	$\tau/\mu\text{s}$
5	469sh, 500 [0.20, 0.40]	11	1.82	0.60	4.89	466 (458) [2.71]	3.88
6	470sh, 501 [0.20, 0.39]	55	2.80	1.96	1.61	469 (459) [2.70]	4.02
7	456sh, 486 [0.18, 0.31]	47	4.15	1.13	1.28	456 (442) [2.81]	5.35
8	452sh, 480 [0.18, 0.27]	52	4.55	1.14	1.05	449sh, 480 (440) [2.82]	5.21

sh = Shoulder. <sup>a</sup> Measured in an integrating sphere under air using an excitation wavelength of 355 nm. <sup>b</sup> Measured at 77 K using an excitation wavelength of 355 nm. <sup>c</sup> Wavelength at 10% intensity on the blue edge of the spectrum obtained at 77 K. <sup>d</sup> Estimated using  $E_T = hc/\lambda_{10\% \text{ em}} \cdot \tau = 1/k_{\text{nr}} + k_r$ .

this is suppressed in a PMMA matrix, it is evident that the dominant pathway for non-radiative decay in solution likely involves significant molecular motion, rather than any other process, for example C–C bond stretching.<sup>47</sup> There are examples of homo- and heteroleptic monoiridium complexes functionalised with bulky 1,2-diarylimidazole ligands that are highly emissive in solution,<sup>34,37,41</sup> which indicates that the bridging ligands of 5–8 are likely to be the structural feature responsible for their non-emissive behaviour in solution. Therefore, we conclude that non-radiative decay through motion of the bridging ligand is responsible for the quenching of solution phosphorescence, which is reinforced by literature precedents.<sup>13,14</sup> There is precedent from work on other diiridium complexes that a rigid polymer matrix such as the cycloolefin polymer zeonex could also lead to a similar emission enhancement.<sup>17</sup>

This property could be anticipated for complex 5 which does not feature rigidifying intramolecular interactions to restrict bridge motion.<sup>13,26,48,49</sup> However, it is more surprising for 6–8, for which intramolecular  $\pi$ – $\pi$  interactions are observed in their solution <sup>19</sup>F NMR spectra (Fig. 3) (similar to complex 4, Fig. 1). The non-emissive nature of complexes 6–8 in solution could be related to their high triplet energies ( $E_T$ ) ( $\geq 2.70$  eV), as we have previously noted that intramolecular  $\pi$ – $\pi$  interactions become less effective at suppressing the non-radiative decay of hydrazide-bridged diiridium complexes in solution as their emission energies increase.<sup>26</sup>

The emission spectra of 5–8 at 77 K in 2-MeTHF are relatively broad and show distinct vibronic features. Minimal rigidochromic shifts are observed on cooling ( $\leq 3$  nm) compared to the room temperature emission spectra recorded in PMMA. This implies a strong LC contribution to the excited states of 5–8.<sup>50</sup> The Huang–Rhys factors ( $S_M$ ) (estimated from the ratio of the  $\nu_{0,0}$  and  $\nu_{0,1}$  band intensities<sup>51,52</sup>) are also large: 5 = 0.8, 6 = 0.8, 7 = 1.0 and 8 > 1.0 (1 s.f.). These values imply that the excited states of 5–8 are highly distorted compared to their ground states,<sup>45</sup> and are related to their non-emissive properties in solution. Comparing these data with those obtained for previous complexes,<sup>13,26</sup> there is a rational inverse relationship between the Huang–Rhys factor and the solution PLQY for hydrazide-bridged diiridium complexes. Complexes with  $S_M$  values of <0.5 (e.g. complex 4) tend to be highly emissive (PLQY =  $\geq 50\%$ ), those that are non-emissive in solution (e.g.

5–8) have  $S_M$  values  $\geq 0.7$ , and those that are weakly emissive (PLQY = ca. 1–5%) have intermediary  $S_M$  values of 0.5–0.7.

The PLQY of 5 in PMMA is notably lower than for 6–8 (11  $\pm$  10% vs. ca. 50  $\pm$  10%). This is ascribed to an absence of rigidifying intramolecular  $\pi$ – $\pi$  interactions in 5 as its  $k_{\text{nr}}$  value is notably large (4.89 vs.  $1.61 \times 10^5 \text{ s}^{-1}$  for 6). The phosphorescence lifetimes of 6–8 are long for blue-green iridium phosphors.<sup>53–57</sup> For example, while 6 has a very similar  $E_T$  to the Hppy-derived complex 4 (2.70 vs. 2.72 eV) and a similar PLQY in PMMA (55 vs. 65  $\pm$  10%), its  $\tau$  is over twice as long (2.80  $\mu\text{s}$  for 6 vs. 1.19  $\mu\text{s}$  for 4). This is related to the substantially lower  $k_r$  of 6 ( $1.96 \times 10^5 \text{ s}^{-1}$  vs.  $5.46 \times 10^5 \text{ s}^{-1}$  for 4) which is likely a consequence of a lower MLCT contribution to the excited state of 6. Therefore, the long phosphorescence lifetimes and low radiative rates of 5–8 are likely to stem from high LC contributions to their excited states. This is evident from the well-resolved vibronic features in their emission spectra recorded in PMMA at room temperature: the  $\nu_{0,0}$ ,  $\nu_{0,1}$ ,  $\nu_{0,2}$  and  $\nu_{0,3}$  bands are all reasonably well-resolved. This conclusion is also supported by minimal rigidochromic shifts in the emission spectra of 5–8 upon cooling (mentioned above). Blue shifting the emission in the series 6–8 through fluorination of the cyclometalating ligands of 7 and 8 also leads to incremental increases in  $\tau$  (i.e. for 8  $\tau = 4.55 \mu\text{s}$  and  $k_r = 1.96 \times 10^5 \text{ s}^{-1}$ ). This fits a typical trend in Ir(III) phosphors, where the LC character of the excited state increases upon blue shifting the emission.<sup>29,58,59</sup>

Complexes 5–8 are emissive under UV irradiation (365 nm) in the solid state as powders. Typical aggregation-induced phosphorescent emission (AIPE) behaviour<sup>47,60</sup> is observed by titrating water into THF solutions of the complexes to induce precipitation/aggregation, which promotes emission. The emission intensity increases as the THF fraction decreases. Spectra for complexes 6 and 8 are shown in Fig. 7. Spectra for 5 and 7 are included in Fig. S3.† The mechanism which results in solid state emission from 5–8 is, in principle no different from that which promotes emission in dilute PMMA films, as evident from near-identical spectral profiles. In the solid state intramolecular motion is restricted due to interactions between neighbouring complexes, rather than between the complexes and a PMMA host. This property is enabled by the bulky (and ancillary – see DFT below) mesityl groups. In the solid state they increase the distances between the emissive

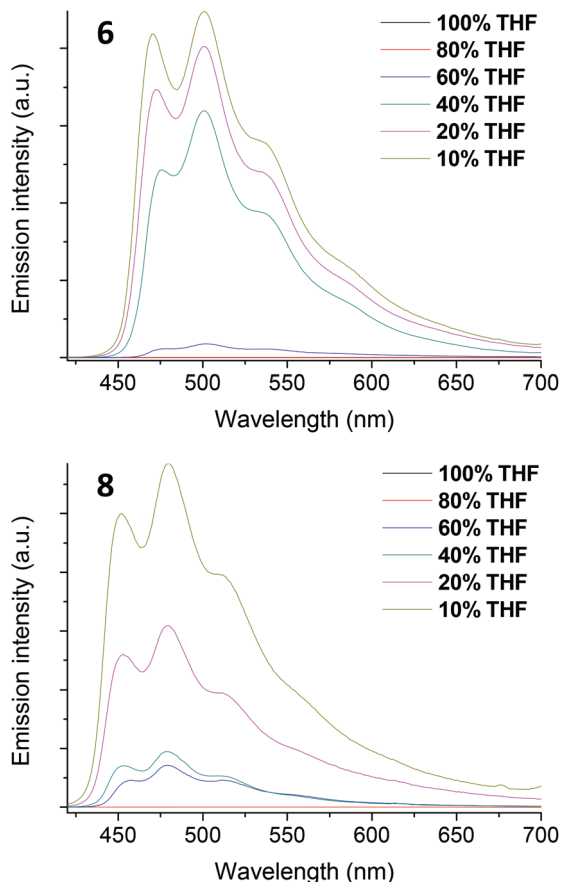


Fig. 7 Emission spectra for THF solutions of complexes **6** and **8** upon incremental titration of water to induce precipitation ( $\lambda_{\text{exc}}$  355 nm). THF fraction is percentage volume.

'cores' of the complexes, suppressing triplet-triplet annihilation as a quenching pathway (which dominates for unshielded diiridium complexes<sup>13,61,62</sup>). Complexes **5–8** greatly extend the spectral range of diiridium AIPE emitters – the most prominent literature examples are orange/red<sup>14,23</sup> while **8** is sky-blue ( $\text{CIE}_{xy} = 0.18, 0.27$  in PMMA).

### Computational study

Electronic structure calculations were carried out on **5–8** at the B3LYP/LANL2DZ:3–21G\* level<sup>12,13,19,26</sup> to gain insight into the photophysical properties of the complexes. In the optimised structures of **5–8** the central hydrazide fragments are predicted to be close to planar for both the *meso* and *rac* diastereomers. This contrasts with previously reported analogues,<sup>12,13,26</sup> for which the *rac* forms tend to be folded, and is assigned to the highly congested nature of the structures. The optimised structures of *meso* **7** and *meso* **8** are in good agreement with the X-ray data. However, the optimised geometries of the *rac* forms of **5–8** cannot be compared with X-ray data as no *rac* structures have been solved. Such similar optimised geometries for the *rac* and *meso* diastereomers of **6–8** may explain why they could not be separated.

The predicted frontier molecular orbital (FMO) contributions are listed in Tables S2 and S3.† Generally, there is a good agreement between diastereomers, and so FMO plots for *meso* **5–8** are presented in Fig. 8 (the FMO plots for the *rac* diastereomers are included in Fig. S4 and S5†). For the diastereomers of **5**, the HOMOs are primarily localised on the Ir centres and the cyclometalating ligands, with some contribution from the central hydrazide fragments of the bridging ligands, while the LUMOs are cyclometalating ligand-based. The spatial separation of the FMOs on the cyclometalating ligands is less defined than for typical Hppy-based complexes,<sup>45,52,63</sup> *i.e.* the LUMO contribution is split nearly equally between the phenyl and imidazole moieties. This is in good agreement with studies on mononuclear complexes with similar 1,2-diarylimidazole cyclometalating ligands.<sup>40–42</sup>

For **6–8** the HOMOs are mainly localised on the Ir centres and the central hydrazide fragments of the bridging ligands. Interestingly, rather than being based on the cyclometalating ligands, the LUMOs are primarily localised on the bridge pentafluorophenyl groups for **6–8**. This contrasts with the data reported for Hppy-based analogues such as **4**, for which the pentafluorophenyl groups are ancillary.<sup>26</sup> Presumably, this is due to the more electron rich nature of the imidazole heterocycles compared to pyridine, which forces the LUMO onto the strongly electron accepting pentafluorophenyl groups. As a result, the cyclometalating ligands of **6–8** are not major FMO contributors (their HOMO and LUMO contributions are

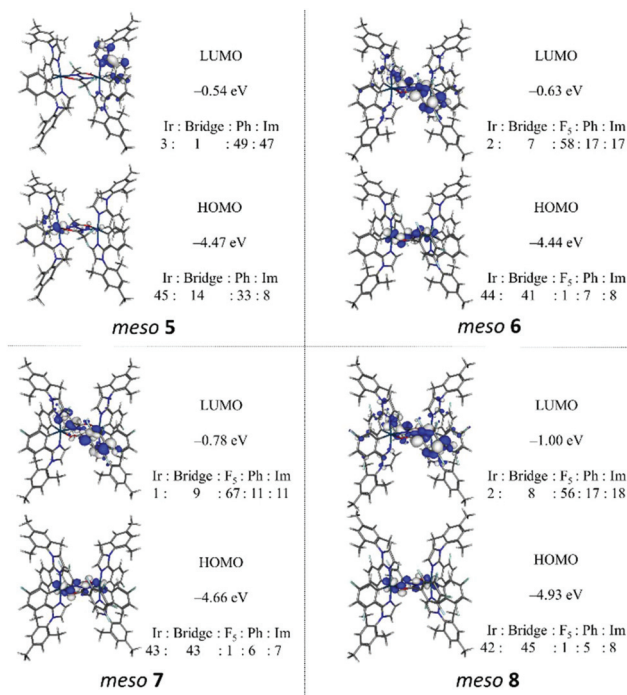


Fig. 8 Molecular orbital compositions for *meso* **5–8**. The orbital contributions are percentages and the HOMO and LUMO energies were calculated at B3LYP/LANL2DZ:3–21G\*. Bridge = central bridge OCNNCO fragment; F<sub>5</sub> = fluorinated bridge aryl rings; Ph = cyclometalating ligand phenyl groups; Im = cyclometalating ligand imidazolyl groups.

Table 4 Summary of the TD-DFT data for complexes 6 and 8

Transition	6				8			
	<i>meso</i>		<i>rac</i>		<i>meso</i>		<i>rac</i>	
	Main orbital contribution	$\lambda$ /nm	Main orbital contribution	$\lambda$ /nm	Main orbital contribution	$\lambda$ /nm	Main orbital contribution	$\lambda$ /nm
$S_0 \rightarrow T_1$	HOMO $\rightarrow$ LUMO	429	HOMO-1 $\rightarrow$ LUMO+3, HOMO $\rightarrow$ LUMO+1	426	HOMO $\rightarrow$ LUMO	420	HOMO-1 $\rightarrow$ LUMO+3	409
$S_0 \rightarrow T_2$	HOMO-2 $\rightarrow$ LUMO+3, HOMO $\rightarrow$ LUMO+1	425	HOMO-1 $\rightarrow$ LUMO+1, HOMO $\rightarrow$ LUMO+3	425	HOMO $\rightarrow$ LUMO+1	410	HOMO-1 $\rightarrow$ LUMO+2, HOMO $\rightarrow$ LUMO+3	409
$S_0 \rightarrow T_3$	HOMO $\rightarrow$ LUMO+3, HOMO-2 $\rightarrow$ LUMO+2	423	HOMO-1 $\rightarrow$ LUMO+4, HOMO-2 $\rightarrow$ LUMO+1	417	HOMO $\rightarrow$ LUMO+3, HOMO-2 $\rightarrow$ LUMO+1	408	HOMO-1 $\rightarrow$ LUMO+4, HOMO-2 $\rightarrow$ LUMO+5	403
$S_0 \rightarrow T_4$	HOMO-1 $\rightarrow$ LUMO+2	416	HOMO-2 $\rightarrow$ LUMO+4	417	HOMO-1 $\rightarrow$ LUMO+4, HOMO-2 $\rightarrow$ LUMO+2	402	HOMO-2 $\rightarrow$ LUMO+4	403
$S_0 \rightarrow T_5$	HOMO-1 $\rightarrow$ LUMO+4	415	HOMO $\rightarrow$ LUMO+17	413	HOMO-1 $\rightarrow$ LUMO+2, HOMO-2 $\rightarrow$ LUMO+4	401	HOMO $\rightarrow$ LUMO+8	402

( $\leq 20\%$ ). Nevertheless, complexes 6–8 are emissive despite their unusual FMO distributions, highlighting the versatility of hydrazide bridges as a platform for obtaining emissive diiridium complexes.

To determine the significance of the unusual FMO distributions of 6–8, a time-dependent density functional theory (TD-DFT) study was carried out to gain insight into the nature of their lowest energy excited states. This is because a simple consideration of the FMOs is not necessarily sufficient to predict the localisation of the lowest energy triplet states of Ir(III) complexes.<sup>64–66</sup> The data for both diastereomers of the least (6) and most (8) fluorinated derivatives are presented in Table 4 (the data for 7 show the same trends and are included in Table S4†). The two largest contributing transitions to each state ( $\geq ca.$  20%) are included. The TD-DFT data for 5 are included in Table S4.†

Both diastereomers of 6–8 feature 5 triplet states that are relatively close in energy ( $\leq 20$  nm). A number of these states may, therefore, be relevant when considering their emissive states.<sup>64</sup> Such a large number of near-degenerate states, many of which have significant contributions from multiple transitions, complicates detailed analysis of the data. However, it can be noted that as well as a HOMO  $\rightarrow$  LUMO transition, many of the relevant transitions in Table 4 involve contributions from higher energy unoccupied (LUMO+1–LUMO+3), and lower energy occupied (HOMO-1 and HOMO-2) orbitals. Contributions for the HOMO-5–LUMO+5 orbitals are tabulated in Tables S2 and S3.† Particularly, while the LUMO+2 and LUMO+3 orbitals of 6–8 generally include a degree of pentafluorophenyl character, their cyclometalating ligand character is much higher than for the LUMOs ( $\geq 50\%$ , as high as 100%). Also, the HOMO-1 and HOMO-2 orbitals for 6–8 are almost exclusively distributed between the Ir atoms and cyclometalating ligands (*ca.* 50 : 50 in all cases), in contrast to the HOMO orbitals that are mainly Ir and hydrazide based. Therefore, while it is likely that the pentafluorophenyl substituents are somewhat involved in the excited states of 6–8, TD-DFT predicts that the cyclometalating ligands are more involved in their emitting states than is implied by a simple

FMO analysis.<sup>35,40</sup> This analysis is in agreement with the photophysical data above. For example, the observation that the profiles of the PL spectra for 6–8 are very similar to those of homoleptic 2-phenylimidazole complexes<sup>30,33–38</sup> (which do not feature bridging ligands) signifies that their excited states should possess a high degree of LC character on the cyclometalating ligands.

## Conclusions

A new family of hydrazide-bridged diiridium complexes 5–8 based on bulky 1,2-diarylimidazole cyclometalating ligands has been studied in detail.

The complexes 6–8 are strongly emissive when doped into PMMA. Significantly emissive ppy-free diiridium complexes are rare, and of these 6–8 exhibit the highest PLQYs yet reported ( $\Phi_{PL} = 47\text{--}55 \pm 10\%$ ).<sup>23,31</sup> They display emission peaks as blue shifted as 452 nm and complex 8 has CIE<sub>xy</sub> colour coordinates in the sky-blue region (0.18, 0.27). Prior to this work there have been only two reports of sky-blue diiridium complexes,<sup>22,26</sup> both containing Hppy ligands. We have shown, therefore, that Hppy is not essential for obtaining highly emissive diiridium complexes, and also Hppy is not required for the challenging task of shifting their emission into the sky-blue region. Moreover, complex 8 is as blue as the bluest mono-Ir complexes yet reported based on arylimidazole ligands.<sup>35,38</sup>

X-ray crystallography and solution-state <sup>19</sup>F NMR spectra reveal the presence of rigidifying intramolecular  $\pi$ - $\pi$  interactions for complexes 6–8, which explains their improved PLQYs compared to 5. The rather long phosphorescence lifetimes of 6–8 have been attributed to the high <sup>3</sup>LC character of their excited states, which is corroborated by TD-DFT.

The complexes also display AIPE behaviour. This substantially broadens the colour range that can now be accessed by AIPE diiridium emitters towards the sky-blue and should provide added versatility in applications such as anti-counterfeiting.<sup>67</sup> This study considerably increases the scope of dinuc-

lear Ir(III) complexes to include luminophoric ligands that are not restricted to Hppy-type cyclometalates, and provides a foundation for further diversification of emissive diiridium complexes away from conventional Hppy architectures.

## Conflicts of interest

There are no conflicts to declare.

## Acknowledgements

We thank EPSRC for funding equipment used in this study (grant EP/K0394/23/1).

## Notes and references

- Iridium(III) in Optoelectronic and Photonics Applications*, ed. E. Zysman-Colman, John Wiley & Sons, Chichester, 2017.
- Y. Chi and P.-T. Chou, *Chem. Soc. Rev.*, 2010, **39**, 638–655.
- Z. Q. Chen, Z. Q. Bian and C. H. Huang, *Adv. Mater.*, 2010, **22**, 1534–1539.
- M. S. Lowry and S. Bernhard, *Chem. – Eur. J.*, 2006, **12**, 7970–7977.
- K. K.-W. Lo, K. H.-K. Tsang, K.-S. Sze, C.-K. Chung, T. K.-M. Lee, K. Y. Zhang, W.-K. Hui, C.-K. Li, J. S.-Y. Lau, D. C.-M. Ng and N. Zhu, *Coord. Chem. Rev.*, 2007, **251**, 2292–2310.
- R. Gao, D. G. Ho, B. Hernandez, M. Selke, D. Murphy, P. I. Djurovich and M. E. Thompson, *J. Am. Chem. Soc.*, 2002, **124**, 14828–14829.
- X. Yang, G. Zhou and W.-Y. Wong, *Chem. Soc. Rev.*, 2015, **44**, 8484–8575.
- C. Ulbricht, B. Beyer, C. Friebe, A. Winter and U. S. Schubert, *Adv. Mater.*, 2009, **21**, 4418–4441.
- T. Hajra, A. J. K. Bera and V. Chandrasekhar, *Aust. J. Chem.*, 2011, **64**, 561–566.
- A. M. Prokhorov, A. Santoro, J. A. G. Williams and D. W. Bruce, *Angew. Chem., Int. Ed.*, 2012, **51**, 95–98.
- M. Graf, R. Czerwieniec and K. Sünkel, *Z. Anorg. Allg. Chem.*, 2013, **639**, 1090–1094.
- Y. Zheng, A. S. Batsanov, M. A. Fox, H. A. Al-Attar, K. Abdullah, V. Jankus, M. R. Bryce and A. P. Monkman, *Angew. Chem., Int. Ed.*, 2014, **53**, 11616–11619.
- D. G. Congrave, Y. Hsu, A. S. Batsanov, A. Beeby and M. R. Bryce, *Organometallics*, 2017, **36**, 981–993.
- G. Li, Y. Wu, G. Shan, W. Che, D. Zhu, B. Song, L. Yan, Z. Su and M. R. Bryce, *Chem. Commun.*, 2014, **50**, 6977–6980.
- P.-H. Lanoë, C. M. Tong, R. W. Harrington, M. R. Probert, W. Clegg, J. A. G. Williams and V. N. Kozhevnikov, *Chem. Commun.*, 2014, **50**, 6831–6834.
- V. Chandrasekhar, T. Hajra, J. K. Bera, S. M. W. Rahaman, N. Satumtira, O. Elbjairami and M. A. Omary, *Inorg. Chem.*, 2012, **51**, 1319–1329.
- R. E. Daniels, S. Culham, M. Hunter, M. C. Durrant, M. R. Probert, W. Clegg, J. A. G. Williams and V. N. Kozhevnikov, *Dalton Trans.*, 2016, **45**, 6949–6962.
- X. Yang, Z. Feng, J. Zhao, J.-S. Dang, B. Liu, K. Zhang and G. Zhou, *ACS Appl. Mater. Interfaces*, 2016, **8**, 33874–33887.
- A. M'hamedi, M. A. Fox, A. S. Batsanov, H. A. Al-Attar, A. P. Monkman and M. R. Bryce, *J. Mater. Chem. C*, 2017, **5**, 6777–6789.
- M. Y. Wong, G. Xie, C. Tourbillon, M. Sandroni, D. B. Cordes, A. M. Z. Slawin, I. D. W. Samuel and E. Zysman-Colman, *Dalton Trans.*, 2015, **44**, 8419–8432.
- G. Li, D. G. Congrave, D. Zhu, Z. Su and M. R. Bryce, *Polyhedron*, 2018, **140**, 146–157.
- J. L. Liao, P. Rajakannu, P. Gnanasekaran, S. R. Tsai, C. H. Lin, S. H. Liu, C. H. Chang, G. H. Lee, P. T. Chou, Z. N. Chen and Y. Chi, *Adv. Opt. Mater.*, 2018, **6**, 1800083.
- G. Li, W. Guan, S. Du, D. Zhu, G. Shan, X. Zhu, L. Yan, Z. Su, M. R. Bryce and A. P. Monkman, *Chem. Commun.*, 2015, **51**, 16924–16927.
- Y. Jiang, G. Li, D. Zhu, Z. Su and M. R. Bryce, *J. Mater. Chem. C*, 2017, **5**, 12189–12193.
- X. Yang, X. Xu, J. Dang, G. Zhou, C.-L. Ho and W.-Y. Wong, *Inorg. Chem.*, 2016, **55**, 1720–1727.
- D. G. Congrave, Y.-T. Hsu, A. S. Batsanov, A. Beeby and M. R. Bryce, *Dalton Trans.*, 2018, **47**, 2086–2098.
- Y. Im, S. Y. Byun, J. H. Kim, D. R. Lee, C. S. Oh, K. S. Yook and J. Y. Lee, *Adv. Funct. Mater.*, 2017, **27**, 1603007–1603031.
- Y. Chi and P.-T. Chou, *Chem. Soc. Rev.*, 2010, **39**, 638–655.
- J. Li, P. I. Djurovich, B. D. Alleyne, M. Yousufuddin, N. N. Ho, J. C. Thomas, J. C. Peters, R. Bau and M. E. Thompson, *Inorg. Chem.*, 2005, **44**, 1713–1727.
- J. Zhuang, W. Li, W. Wu, M. Song, W. Su, M. Zhou and Z. Cui, *New J. Chem.*, 2015, **39**, 246–253.
- G. Li, X. Ren, G. Shan, W. Che, D. Zhu, L. Yan, Z. Su and M. R. Bryce, *Chem. Commun.*, 2015, **51**, 13036–13039.
- R. Davidson, Y.-T. Hsu, T. Batchelor, D. Yufit and A. Beeby, *Dalton Trans.*, 2016, **45**, 11496–11507.
- J. Zhuang, W. Li, W. Su, Y. Liu, Q. Shen, L. Liao and M. Zhou, *Org. Electron.*, 2013, **14**, 2596–2601.
- K. Udagawa, H. Sasabe, C. Cai and J. Kido, *Adv. Mater.*, 2014, **26**, 5062–5066.
- H. Cho, J. Lee, J. I. Lee, N. S. Cho, J. H. Park, J. Y. Lee and Y. Kang, *Org. Electron.*, 2016, **34**, 91–96.
- Y. Zhang, J. Lee and S. R. Forrest, *Nat. Commun.*, 2014, **5**, 1–7.
- K. Udagawa, H. Sasabe, F. Igarashi and J. Kido, *Adv. Opt. Mater.*, 2016, **4**, 86–90.
- Y. Kwon, S. H. Han, S. Yu, J. Y. Lee and K. M. Lee, *J. Mater. Chem. C*, 2018, **6**, 4565–4572.
- M. Micksch, M. Tenne and T. Strassner, *Eur. J. Org. Chem.*, 2013, 6137–6145.
- T. Karatsu, M. Takahashi, S. Yagai and A. Kitamura, *Inorg. Chem.*, 2013, **52**, 12338–12350.
- E. Baranoff, S. Fantacci, F. De Angelis, X. Zhang, R. Scopelliti, M. Grätzel and M. K. Nazeeruddin, *Inorg. Chem.*, 2011, **50**, 451–462.

- 42 S. Takizawa, J. Nishida, T. Tsuzuki, S. Tokito and Y. Yamashita, *Inorg. Chem.*, 2007, **46**, 4308–4319.
- 43 D. G. Congrave, A. S. Batsanov, M. Du, Y. Liu, D. Zhu and M. R. Bryce, *Inorg. Chem.*, 2018, **57**, 12836–12849.
- 44 C. Hansch, A. Leo and R. W. Taft, *Chem. Rev.*, 1991, **91**, 165–195.
- 45 A. B. Tamayo, B. D. Alleyne, P. I. Djurovich, S. Lamansky, I. Tsyba, N. N. Ho, R. Bau and M. E. Thompson, *J. Am. Chem. Soc.*, 2003, **125**, 7377–7387.
- 46 S. Lamansky, P. Djurovich, D. Murphy, F. Abdel-Razzaq, H. E. Lee, C. Adachi, P. E. Burrows, S. R. Forrest and M. E. Thompson, *J. Am. Chem. Soc.*, 2001, **123**, 4304–4312.
- 47 J. Mei, N. L. C. Leung, R. T. K. Kwok, J. W. Y. Lam and B. Z. Tang, *Chem. Rev.*, 2015, **115**, 11718–11940.
- 48 C. E. Housecroft and E. C. Constable, *Coord. Chem. Rev.*, 2017, **350**, 155–177.
- 49 R. D. Costa, E. Ortí, H. J. Bolink, F. Monti, G. Accorsi and N. Armaroli, *Angew. Chem., Int. Ed.*, 2012, **51**, 8178–8211.
- 50 E. S. Andreiadis, D. Imbert, J. Pécaut, A. Calborean, I. Ciofini, C. Adamo, R. Demadrille and M. Mazzanti, *Inorg. Chem.*, 2011, **50**, 8197–8206.
- 51 G. Li, T. Fleetham, E. Turner, X. C. Hang and J. Li, *Adv. Opt. Mater.*, 2015, **3**, 390–397.
- 52 J. Li, P. I. Djurovich, B. D. Alleyne, M. Yousufuddin, N. N. Ho, J. C. Thomas, J. C. Peters, R. Bau and M. E. Thompson, *Inorg. Chem.*, 2005, **44**, 1713–1727.
- 53 A. F. Henwood, A. K. Bansal, D. B. Cordes, A. M. Z. Slawin, I. D. W. Samuel and E. Zysman-Colman, *J. Mater. Chem. C*, 2016, **4**, 3726–3737.
- 54 C.-H. Yang, M. Mauro, F. Polo, S. Watanabe, I. Muenster, R. Frohlich and L. De Cola, *Chem. Mater.*, 2012, **24**, 3684–3695.
- 55 T. Duan, T.-K. Chang, Y. Chi, J.-Y. Wang, Z.-N. Chen, W.-Y. Hung, C.-H. Chen and G.-H. Lee, *Dalton Trans.*, 2015, **44**, 14613–14624.
- 56 H. J. Park, J. N. Kim, H. Yoo, K. Wee, S. O. Kang and D. W. Cho, *J. Org. Chem.*, 2013, **78**, 8054–8064.
- 57 T. B. Fleetham, L. Huang, K. Klimes, J. Brooks and J. Li, *Chem. Mater.*, 2016, **28**, 3276–3282.
- 58 M. A. Baldo, S. R. Forrest and M. E. Thompson, in *Organic Electroluminescence*, ed. Z. H. Kafafi, CRC and SPIE Press, 2005.
- 59 L. Yang, F. Okuda, K. Kobayashi, K. Nozaki, Y. Tanabe, Y. Ishii and M.-A. Haga, *Inorg. Chem.*, 2008, **47**, 7154–7165.
- 60 L. Ravotto and P. Ceroni, *Coord. Chem. Rev.*, 2017, **346**, 62–76.
- 61 S. Reineke, K. Walzer and K. Leo, *Phys. Rev. B: Condens. Matter Mater. Phys.*, 2007, **75**, 125328.
- 62 N. C. Giebink and S. R. Forrest, *Phys. Rev. B: Condens. Matter Mater. Phys.*, 2008, **77**, 235215.
- 63 H. Benjamin, Y. Zheng, A. S. Batsanov, M. A. Fox, H. A. Al-Attar, A. P. Monkman and M. R. Bryce, *Inorg. Chem.*, 2016, **55**, 8612–8627.
- 64 H. J. Bolink, F. De Angelis, E. Baranoff, C. Klein, S. Fantacci, E. Coronado, M. Sessolo, K. Kalyanasundaram, M. Grätzel and M. K. Nazeeruddin, *Chem. Commun.*, 2009, 4672–4674.
- 65 E. Baranoff and B. F. E. Curchod, *Dalton Trans.*, 2015, **44**, 8318–8329.
- 66 X. Gu, T. Fei, H. Zhang, H. Xu, B. Yang, Y. Ma and X. Liu, *J. Phys. Chem. A*, 2008, **112**, 8387–8393.
- 67 Y. Jiang, G. Li, W. Che, Y. Liu, B. Xu, G. Shan, D. Zhu, Z. Su and M. R. Bryce, *Chem. Commun.*, 2017, **53**, 3022–3025.